A Novel Technology for the Imaging of Acidic Prostate Tumors by Positron Emission Tomography

Amy L. Vāvere,[1] Gráinne B. Biddlecombe,[1] William M. Spees,[2] Joel R. Garbow,[2] Dayanjali Wijesinghe,[3] Oleg A. Andreev,[3] Donald M. Engelman,[4] Yana K. Reshetnyak,[3] and Jason S. Lewis[1,5]

[1]Division of Radiological Sciences and [2]Biomedical MR Laboratory, Department of Radiology, Washington University School of Medicine, St. Louis, Missouri; [3]Physics Department, University of Rhode Island, Kingston, Rhode Island; [4]Department of Molecular Biophysics and Biochemistry, Yale University, New Haven, Connecticut; and [5]Department of Radiology, Memorial Sloan-Kettering Cancer Center, New York, New York

Abstract

Solid tumors often develop an acidic environment due to the Warburg effect. The effectiveness of diagnosis and therapy may therefore be enhanced by the design and use of pH-sensitive agents that target acidic tumors. Recently, a novel technology was introduced to target acidic tumors using pH low insertion peptide (pHLIP), a peptide that inserts across cell membranes as an α-helix when the extracellular pH (pH_e) is acidic. In this study, we expanded the application of the pHLIP technology to include positron emission tomography imaging of the acidic environment in prostate tumors using ^{64}Cu conjugated to the pHLIP (^{64}Cu-DOTA-pHLIP). Studies showed that this construct avidly accumulated in LNCaP and PC-3 tumors, with higher uptake and retention in the LNCaP tumors. Uptake correlated with differences in the bulk pH_e of PC-3 and LNCaP tumors measured in magnetic resonance spectroscopy experiments by the ^{31}P chemical shift of the pH_e marker 3-aminopropylphosphonate. This article introduces a novel class of noninvasive pH-selective positron emission tomography imaging agents and opens new research directions in the diagnosis of acidic solid tumors. [Cancer Res 2009;69(10):4510–6]

Introduction

Studies of the gene signatures of cancer cells indicate that many different genes are either up-regulated or down-regulated, even within a given type of tumor, so it is problematic to rely on any single biomarker for the diagnosis of even a single type of cancer (1). However, physiologic processes (e.g., hypoxia and acidity), which are present in 90% of tumor microenvironments, are considered promising environmental markers for tumor targeting (2, 3). In particular, an acidic tumor environment plays a significant role in tumor progression and is often associated with increased invasion and metastasis (4–6) as well as resistance to drug therapies (5, 7, 8). Recently, a correlation was observed between extracellular pH (pH_e) and overall survival following treatment with combined hyperthermia and radiation therapy for spontaneous sarcomas in canines (9). Tumor pH has practical importance because most anticancer drugs must be transported either by active transport or by passive diffusion into cells, where they frequently undergo further metabolism. As all of these processes might be pH sensitive, the cytotoxic activity of an anticancer drug could depend on both the intracellular pH and the pH_e. In the case of chemotherapeutic agents that are weak acids or bases and enter targeted cells via passive diffusion, it is the nonionized form that crosses the cell membrane. It also has been suggested that modulation of tumor pH, both intracellular pH and pH_e, could be used to increase the uptake of therapeutic drugs (7, 10–12). Delineation of intracellular pH from pH_e is impossible with electrode-based techniques due to the scale of the electrode compared with the tissue. Thus, noninvasive tools for monitoring pH_e and the effectiveness of its modulation could be extremely valuable.

Several magnetic resonance-based methods for the estimation of pH_e in animal tumor models have been introduced in recent years. These approaches include the use of T_1-weighted magnetic resonance imaging with extracellular contrast agents that exhibit pH-dependent ^1H relaxation enhancement (13), ^1H and ^{31}P pH-dependent chemical shift measurements of exogenous extracellular species (14–16), and ^{13}C chemical shift imaging of hyperpolarized ^{13}C-labeled bicarbonate (17). Studies with the ^{31}P pH_e indicator 3-aminopropylphosphonate (3-APP) have confirmed that the average pH_e of tumors is acidic, with values reaching as low as 6.0 (18). At present, however, these techniques cannot be readily translated to the clinic.

Positron emission tomography (PET) is a widely used molecular imaging modality in both clinical and research settings (19). The use of ^{64}Cu as a PET nuclide, and the basis for new radiopharmaceuticals, is particularly attractive given its 12.74 h half-life (20). ^{64}Cu complexes have been studied as PET agents with the nuclide incorporated into either small molecules or peptides (21, 22). Here we present the ^{64}Cu PET imaging of prostate tumors using the recently discovered acid-targeting peptide, pH low insertion peptide (pHLIP; refs. 23–25). The pHLIP contains 37 residues. At neutral pH_e, it interacts with the surface of membranes as an unstructured peptide, but at acidic pH_e (<7.0), it inserts across the membrane and forms a stable transmembrane α-helix (24). We have shown that pHLIP can target a variety of fluorescent dyes conjugated to its NH_2 terminus to a tissue with elevated extracellular acidity *in vivo* and also that it can deliver chemotherapeutics into cells through interactions with the membrane lipid bilayer, avoiding the need for any specific interaction with membrane proteins (23, 25, 26). The present study was undertaken to evaluate whether it is possible to delineate lower pH_e in prostate tumors *in vivo* with ^{64}Cu
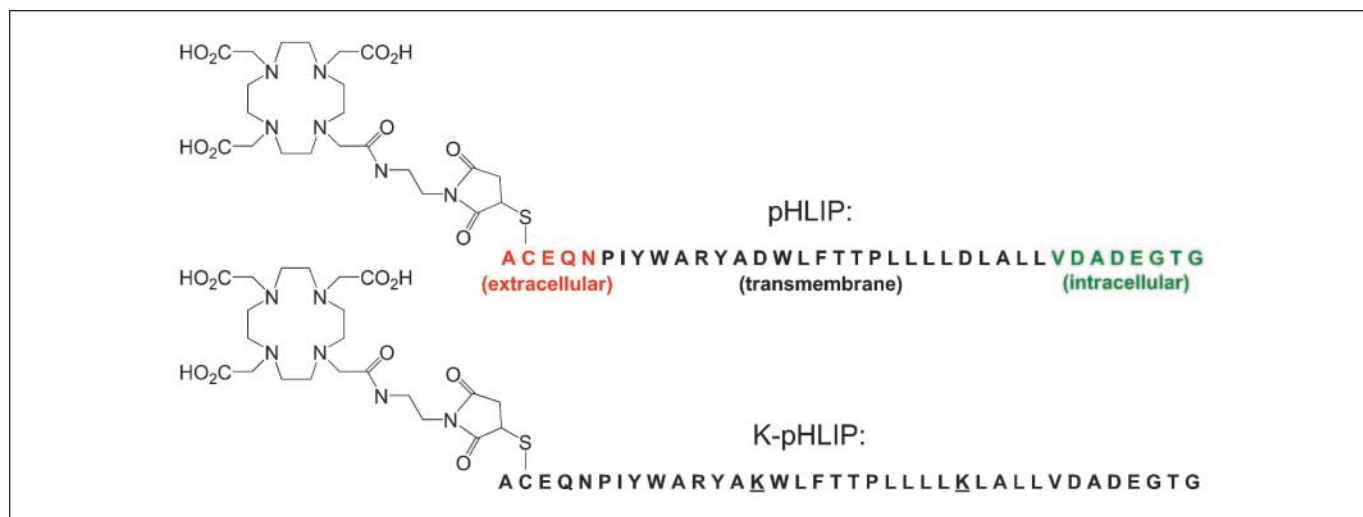
Figure 1. Amino acid sequence of the native peptide compared with the mutant pHLIP (K-pHLIP).

conjugated to the pHLIP (^{64}Cu-DOTA-pHLIP), the first compound of a new generation of novel pH-selective tumor PET imaging agents.

Materials and Methods

All chemicals, unless otherwise stated, were purchased from Sigma-Aldrich. Radioactive samples were counted in a radioisotope calibrator (Capintec) for determination of mCi and an automated-well Beckman 8000 gamma counter (Beckman Coulter) for counts/min. Male athymic *nu/nu* mice were purchased from the National Cancer Institute. Human prostate carcinoma tumor cell lines PC-3 and LNCaP were obtained from the American Type Culture Collection and maintained by serial passage in cell culture.

Preparation of peptides and ^{64}Cu radiolabeling. All peptides were prepared by solid-phase peptide synthesis using standard 9-fluorenylmethyloxycarbonyl chemistry and purified by reverse-phase chromatography (on a C18 column) at the W.M. Keck Foundation Biotechnology Resource Laboratory at Yale University. Peptide sequences were ACEQNPIYWAR-YADWLFTTPLLLLDLALLVDADEGTG (pHLIP) and ACEQNPIYWAR-YA*K*WLFTTPLLLL*K*LALLVDADEGTG (K-pHLIP). The NH$_2$ terminus of the pHLIP was covalently conjugated to 1,4,7,10-tetraazacyclododecane-1,4,7-Tris-acetic acid-10-maleimidoethylacetamide, a maleimide-containing derivative of DOTA, a chelator used for the effective binding of copper radionuclides (27). The peptides were incubated with 2× molar excess of DOTA-maleimide (Macrocyclics) in the presence of 2 mmol/L EDTA in PBS (pH 7.4) overnight at 4°C. Free DOTA-maleimide and EDTA were removed by a Sephadex G-10 spin column equilibrated with PBS (pH 7.4). The concentration of peptide was determined by absorbance at 280 nm using a molar extinction coefficient of ε_{280} = 13,940 mol/L^{-1} cm^{-1}. The composition and degree of conjugation were confirmed by mass spectrometry and high-performance liquid chromatography. The peptides were analyzed by electrospray mass spectrometry [ES+; DOTA-pHLIP: m/z calculated for C$_{215}$H$_{323}$N$_{50}$O$_{66}$S (M$^+$) = 4693.3, found 1174.74 (M + 4H$^+$) and 1565.4 (M + 3H$^+$)]. Reverse-phase high-performance liquid chromatography involved a Waters X-Bridge (C4, 4.6 × 75 mm) column with a gradient [0-2 min 20% B to 40% B, 2-7 min 40% B to 70% B, and 7-10 min 70% B to 100% B (solvent A: 0.01% trifluoroacetic acid in water and solvent B: 0.01% trifluoroacetic acid in acetonitrile)] at a flow rate of 1 mL/min. Detection was accomplished at 280 nm and the retention times for DOTA-pHLIP and DOTA-K-pHLIP were 5.45 and 4.82 min, respectively. The peptides were stored at −80°C.

^{64}Cu was produced at Washington University School of Medicine and processed by previously reported literature methods (28). Maximal labeling for both constructs was achieved in 0.5 mol/L ammonium acetate (pH 5.5) at 25°C for 30 min at a ratio of 1:1 (μg:mCi). Before purification, 5 mmol/L

EDTA was added to scavenge any uncomplexed ^{64}Cu. Purification was achieved by C18 SepPak Light using 100% ethanol as the eluent. Purity and labeling efficiency were determined by radio-TLC on silica using 10% ammonium acetate/methanol (50:50).

Acute biodistribution. All animal experiments were done in compliance with the Guidelines for the Care and Use of Research Animals established by Washington University Animal Studies Committee. Male athymic mice (20-25 g; National Cancer Institute) were implanted in the right flank with either 1 × 10^7 PC-3 or LNCaP human prostate adenocarcinoma cells in 100 μL cell medium with >90% viability. The LNCaP cells were implanted using Matrigel (BD Biosciences). Tumors were allowed to grow to ~0.5 to 0.75 cm^3 in volume. Mice were randomized before the study. To investigate specific uptake of tumor, organ, and other nontarget tissues, a small amount of ^{64}Cu-DOTA-pHLIP (~28 μCi, 0.22 μg) was injected intravenously into each of the mice bearing palpable PC-3 or LNCaP tumors. The animals were sacrificed at selected time points after injection (1, 4, 24, and 48 h; n = 4-5) and desired tissues were removed, weighed, and counted for radioactivity accumulation. The %ID/g and %ID/organ were calculated by comparison with a weighed, counted standard solution. An additional group of PC-3 mice were injected with ^{64}Cu-DOTA-K-pHLIP (~28 μCi, 0.22 μg) and sacrificed at 1 h (n = 5). Due to a technical error, an additional group of mice were injected and just the kidneys were removed. Because the aspartic acid residues have been changed to lysines in the transmembrane portion, the K-pHLIP should not have the ability to form an α-helix and span the membrane of the cells in acidic environments. On a different day, an additional cohort of LNCaP-bearing mice (which were implanted with a different passage of LNCaP cells; n = 8) were split into two groups, with the first group receiving 150 mmol/L bicarbonated water at pH 8.0 (3.1455 g sodium bicarbonate dissolved in 250 mL drinking water) *ad libitum* for 7 days before the acute biodistribution study (4 h) to modulate tumor pH$_e$ (12, 25, 29) and the second group receiving regular drinking water. Magnetic resonance spectroscopy (MRS) studies were done on the tumors in all of these mice before biodistribution.

Small-animal PET. Imaging ^{64}Cu-DOTA-pHLIP was done on two tumor models using a microPET-F220 (30). Imaging was done in 10 min static sessions, with a collection of 600 frames per session. Isoflurane (2%) was used as an inhaled anesthetic to induce and maintain anesthesia during imaging. Male athymic mice were implanted in the right flank with PC-3 (n = 4) or LNCaP (n = 10) human prostate adenocarcinoma cells, which were allowed to grow until palpable. At this point, the mice were injected intravenously with 200 μCi ^{64}Cu-DOTA-pHLIP and then imaged in pairs at 1, 4, and 24 h post-injection. Images

were reconstructed by Fourier rebinning followed by two-dimensional Ordered Subset Expectation Maximization. Small-animal PET images were evaluated by analysis of the standardized uptake value (SUV) of the tumor and muscle using the software ASIPRO (Concorde MicroSystems). The average radioactivity concentration within the tumor or tissue was obtained from the average pixel values reported in nCi/mL within a volume of interest drawn around the entire tumor or tissue on multiple, consecutive transaxial image slices. SUVs were calculated by dividing this value, the decay-corrected activity per unit volume of tissue (nCi/mL), by the injected activity per unit of body weight (nCi/g).

MRS. *In vivo* pH_e was determined in LNCaP and PC-3 tumors within the 24 h period immediately before injection of ^{64}Cu-labeled pHLIP. Noninvasive measurements of pH_e were based on the ^{31}P magnetic resonance-observable chemical shift of 3-APP (31). Before magnetic resonance measurements, mice bearing PC-3 ($n = 3$) or LNCaP ($n = 6$) tumors were anesthetized with isoflurane and maintained on isoflurane/O_2 (1.25% v/v) throughout data collection. Each anesthetized mouse received an intraperitoneal injection of 0.35 mL 3-APP (Sigma-Aldrich) solution prepared at a concentration of 75 mg 3-APP/mL in isotonic saline. After injection, mice were placed in a head holder with a nose cone for delivery of anesthetic gas and a custom-built ^{31}P magnetic resonance surface coil was placed around the tumor.

^{31}P magnetic resonance studies were done using a small-animal magnetic resonance scanner based on a Magnex Scientific Instruments 11.74 T (^{31}P resonance frequency 202.3 MHz), 26 cm horizontal-bore magnet interfaced with a Varian NMR Systems INOVA console. Magnetic field homogeneity was optimized by shimming on the free induction decay of the tumor water resonance, observed through the ^{31}P magnetic resonance surface coil. ^{31}P spectral acquisition parameters were: sweep width of 20,000 Hz, 0.3 s acquisition time, 4.06 s repetition time, and a 60° excitation pulse. A total of 512 transients were averaged for each measurement; thus, the total length of each ^{31}P scan was 34 min. Magnetic resonance data were processed with a matched filter (30 Hz line-broadening) and frequency estimates for the ^{31}P MRS components were done using a Bayesian Probability Theory analysis package developed at Washington University (32). The resulting estimated chemical shift difference between 3-APP and the pH-independent α-nucleoside triphosphate resonance (33) was used to determine pH_e based on the fitting parameters provided by Gillies and colleagues (31).

Statistics. Statistically significant differences between mean values were determined using ANOVA coupled to Scheffe's test or, for statistical classification, a Student's t test was done. Differences at the 95% confidence level ($P < 0.05$) were considered significant.
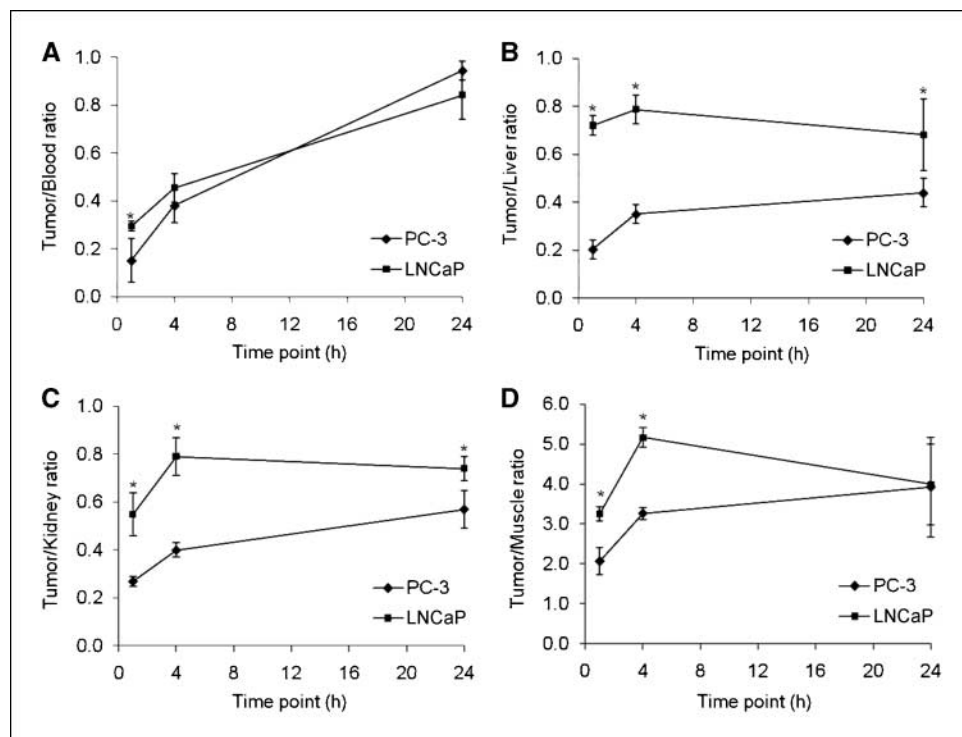
Results

^{64}Cu-DOTA-pHLIP and ^{64}Cu-DOTA-K-pHLIP can be obtained in high yield and good specific activity. ^{64}Cu labeling of DOTA-pHLIP was attempted at various pH values between 4.5 and 9.2

Table 1. Acute biodistribution of ^{64}Cu-DOTA-pHLIP in tissues in PC-3 and LNCaP mice and ^{64}Cu-DOTA-K-pHLIP in PC-3 mice

PC-3	1 h	4 h	24 h	1 h
	^{64}Cu-DOTA-pHLIP	^{64}Cu-DOTA-pHLIP	^{64}Cu-DOTA-pHLIP	^{64}Cu-DOTA-K-pHLIP
Blood	11.27 ± 0.81	7.45 ± 1.76	2.59 ± 0.48	7.09 ± 0.67
Lung	5.16 ± 0.51	4.25 ± 0.94	2.35 ± 0.46	3.75 ± 0.18
Liver	8.56 ± 1.14	7.99 ± 1.28	5.86 ± 1.23	5.21 ± 1.75
Spleen	2.10 ± 0.14	2.02 ± 0.47	1.82 ± 0.44	1.64 ± 0.29
Kidney	6.32 ± 0.39	6.93 ± 0.83	4.64 ± 1.27	4.63 ± 0.35*
Muscle	1.11 ± 0.79	0.86 ± 0.16	0.65 ± 0.14	0.56 ± 0.09
Skin	1.77 ± 0.09	2.07 ± 0.36	1.87 ± 0.33	0.96 ± 0.06
Fat	0.80 ± 0.39	0.86 ± 0.27	0.53 ± 0.18	1.09 ± 0.80
Heart	3.95 ± 0.60	3.17 ± 0.83	1.67 ± 0.14	2.50 ± 0.55
Brain	0.47 ± 0.11	0.35 ± 0.12	0.16 ± 0.04	0.30 ± 0.06
Bone	1.55 ± 0.19	1.17 ± 0.41	0.81 ± 0.14	1.12 ± 0.41
PC-3	1.72 ± 0.17	2.78 ± 0.19	2.46 ± 0.57	1.04 ± 0.15

LNCaP	1 h	4 h	24 h	48 h
	^{64}Cu-DOTA-pHLIP	^{64}Cu-DOTA-pHLIP	^{64}Cu-DOTA-pHLIP	^{64}Cu-DOTA-pHLIP
Blood	14.97 ± 1.11	8.08 ± 0.35	3.96 ± 1.11	1.68 ± 0.35
Lung	5.63 ± 0.62	4.38 ± 0.39	3.22 ± 0.53	2.22 ± 0.70
Liver	6.53 ± 1.02	4.80 ± 0.72	4.88 ± 0.98	4.43 ± 0.74
Spleen	2.75 ± 0.48	2.05 ± 0.09	1.84 ± 0.27	1.41 ± 0.35
Kidney	8.34 ± 0.66	5.42 ± 0.58	4.48 ± 1.08	2.76 ± 0.50
Muscle	1.38 ± 0.53	0.72 ± 0.11	0.85 ± 0.25	0.49 ± 0.10
Skin	4.16 ± 1.72	2.35 ± 0.15	2.87 ± 0.54	1.68 ± 0.20
Fat	2.40 ± 0.73	0.87 ± 0.17	0.60 ± 0.16	0.26 ± 0.14
Heart	5.31 ± 1.03	3.60 ± 0.28	2.02 ± 0.31	1.45 ± 0.08
Brain	0.45 ± 0.06	0.29 ± 0.05	0.24 ± 0.05	0.16 ± 0.04
Bone	3.77 ± 1.88	1.03 ± 0.10	1.00 ± 0.28	0.60 ± 0.10
LNCaP	4.50 ± 1.71	3.67 ± 0.56	3.23 ± 0.55	1.74 ± 1.41

*Due to a technical error, an additional group of mice were used to produce these data. Data are %ID/g ± SD in $n = 4$ to 5 mice per group.

Figure 2. Comparisons of various tumor-to-tissue ratios from ^{64}Cu-DOTA-pHLIP biodistribution data presented in Table 1. Tumor %ID/g was divided by the corresponding %ID/g of the tissue of interest for (*A*) blood, (*B*) liver, (*C*) kidney, and (*D*) muscle. *, *P* < 0.05, statistical significance at the 95% confidence level.

using 0.125 to 0.5 mol/L ammonium acetate. Optimal labeling was achieved in 0.5 mol/L ammonium acetate (pH 5.5) at 25°C for 30 min at a ratio of 1:1 (μg:mCi) at a specific activity of 1,591 mCi/μmol. Without heating, the labeled solution remained stable overnight. Radiochemical purity was consistently >95% following EDTA scavenge and SepPak purification as shown by radio-TLC on silica using 10% ammonium acetate/methanol (50:50). As a control, we used a mutant version of pHLIP (K-pHLIP) in which key Asp residues of the transmembrane part of pHLIP were replaced by positively charged Lys residues (Fig. 1). These changes prevent the peptide from inserting across the cell membrane and forming an α-helix at acidic pH (25). The mutant/control peptide (K-pHLIP) was labeled in a similar manner at a specific activity of 1,713 mCi/μmol at >95% radiochemical purity.

Acute biodistribution of ^{64}Cu-DOTA-pHLIP in PC-3 and LNCaP and ^{64}Cu-DOTA-K-pHLIP in PC-3 tumor-bearing mice. Organ, tissue, and tumor uptake was examined by acute biodistribution studies of ^{64}Cu-DOTA-pHLIP after injection into male nude mice bearing either LNCaP or PC-3 tumors (Table 1). One additional group of PC-3–bearing mice received the equivalent mass of ^{64}Cu-DOTA-K-pHLIP as a control. The PC-3 tumor accumulation of ^{64}Cu-DOTA-pHLIP reached a maximum after 4 h (2.78 ± 0.19%ID/g) and the tumor retention was high, with 2.46 ± 0.57%ID/g remaining at 24 h. In the LNCaP mice, tumor accumulation of ^{64}Cu-DOTA-pHLIP reached a maximum after only 1 h (4.50 ± 1.71%ID/g) and the tumor retention was also high, with 3.23 ± 0.55%ID/g remaining at 24 h and 1.74 ± 1.41%ID/g at 48 h post-injection. The biodistribution data for ^{64}Cu-DOTA-pHLIP showed that the radioactive background in the blood and blood-rich organs, such as liver, lung, heart, and spleen, was similar in the two tumor models, whereas differences were noted in the tumors. Examination of tumor-to-tissue ratios (Fig. 2) clearly shows that, for imaging purposes, the 4 h time point is optimal for both tumor models. This can be attributed to better retention of the agent in

tumor tissue and more rapid washout of activity from background organs.

The administration of the mutant peptide, ^{64}Cu-DOTA-K-pHLIP, resulted in a ~40% lower PC-3 tumor accumulation at 1 h post-injection, which is impressive in that the subsequent MRS study showed the PC-3 tumors to be less acidic. However, distribution of the control peptide, ^{64}Cu-DOTA-K-pHLIP, was similar in pattern to the parent, ^{64}Cu-DOTA-pHLIP, although with a reduction in accumulation in all tissues. The most likely reason for this universal reduction is a more rapid excretion of the mutant-pHLIP, which has been observed by fluorescence imaging as well, and, as a consequence, less retention in the blood and therefore the tissues. Our biophysical studies indicate that pHLIP binds to the surfaces of membranes at normal pH (26), which might lead to the slow kinetics of peptide distribution *in vivo*. Most probably, the mutant pHLIP has reduced binding affinity to the membrane and, therefore, a faster kinetic profile. It is important to note that the mutant peptide was not taken up to the same extent by the skin or the kidney, which are tissues known to be more acidic than all other healthy tissues and organs.

The final groups of animals studied were LNCaP-bearing mice that were given either normal drinking water or water spiked with sodium bicarbonate to modulate the tumor pH$_e$. As shown by MRS, the bicarbonate water resulted in the modulated tumor having a more basic pH$_e$ (see below). The results of the biodistribution in these mice (Table 2) were similar to those for LNCaP tumors presented in Table 1, but it is important to note that these studies were done on different dates with mice that had been implanted with a different passage of LNCaP cells. Except for uptake in the tumor and kidney, no significant differences were observed between the two groups in the 17 collected organs and tissues. ^{64}Cu-DOTA-pHLIP uptake in the nonmodulated LNCaP tumors was "greater" than the uptake in the tumors in mice that received

7 days of bicarbonated water (4.50 ± 1.71 versus 1.31 ± 0.60, respectively; $P = 0.005$).

Small-animal PET imaging of ^{64}Cu-DOTA-pHLIP in PC-3 and LNCaP prostate tumors. Delineation of the tumor by uptake of ^{64}Cu-DOTA-pHLIP was evident in both tumor models (Fig. 3) but to a greater extent in the LNCaP-bearing mice, whereas ^{64}Cu-DOTA-K-pHLIP did not exhibit any targeting ability (data not shown). In the PC-3 model, the tumor-to-muscle ratios derived from the SUVs for uptake of native peptide at 1, 4, and 24 h were 1.45 ± 0.09, 2.67 ± 0.40, and 4.64 ± 1.08, showing a gradual increase in tumor uptake with concurrent washout from nontarget organs. The tumor-to-muscle ratios derived from the SUVs in the LNCaP tumor model were significantly higher ($P = 0.0001$), with values of 3.44 ± 0.50, 5.56 ± 0.21, and 6.55 ± 1.98 for the 1, 4, and 24 h time points, respectively.

MRS directly measures the volume-average pH$_e$ of tumors. The acute biodistribution data and imaging results presented above show higher uptake and retention of ^{64}Cu-DOTA-pHLIP in the nonalkalinized LNCaP tumors and suggest that the pH$_e$ of LNCaP tumors is more acidic than that of PC-3 tumors. To determine tumor-average pH$_e$ directly, ^{31}P MRS measurements with the exogenous pH$_e$ marker 3-APP were used (Fig. 4). PC-3 and LNCaP tumor models were selected for pH measurements based on their significantly different SUVs as measured by PET, with LNCaP showing more uptake of the pHLIP than PC-3. This difference was mirrored in the pH values determined by magnetic resonance, with the LNCaP tumors showing a significantly more acidic average pH$_e$ (6.78 ± 0.29) when compared with the PC-3 tumors (7.23 ± 0.10; $P = 0.039$). Additional evidence that the ^{64}Cu-DOTA-pHLIP targeted pH$_e$ was provided in the study in LNCaP tumors in which half of the mice were fed bicarbonated water before the biodistribution.

Table 2. Acute biodistribution in LNCaP-bearing mice split into two groups: (*a*) mice that received 150 mmol/L bicarbonated water at pH 8.0 *ad libitum* for 7 d before the study and (*b*) mice fed regular drinking water

	4 h (untreated)	4 h (modulated)
Blood	7.21 ± 1.39	7.27 ± 1.00
Lung	3.63 ± 0.63	3.85 ± 0.61
Liver	5.29 ± 1.64	5.79 ± 0.66
Spleen	1.49 ± 0.32	1.53 ± 0.25
Kidney*	5.20 ± 1.06	3.78 ± 0.29
Muscle	0.69 ± 0.40	1.05 ± 0.80
Skin	1.12 ± 0.29	1.02 ± 0.27
Fat	1.26 ± 1.42	1.16 ± 0.50
Heart	2.07 ± 0.28	2.39 ± 0.44
Brain	0.59 ± 0.69	0.27 ± 0.06
Bone	1.22 ± 1.15	2.22 ± 2.51
Pancreas	1.48 ± 0.77	1.56 ± 0.67
Stomach	0.88 ± 0.58	1.01 ± 0.26
Small intestine	2.05 ± 1.04	2.48 ± 0.59
Upper large intestine	2.35 ± 1.25	3.55 ± 1.94
Lower large intestine	1.28 ± 0.79	1.23 ± 0.54
LNCaP*	4.50 ± 1.71	1.31 ± 0.60

NOTE: Data are %ID/g ± SD in $n = 4$ mice per group.
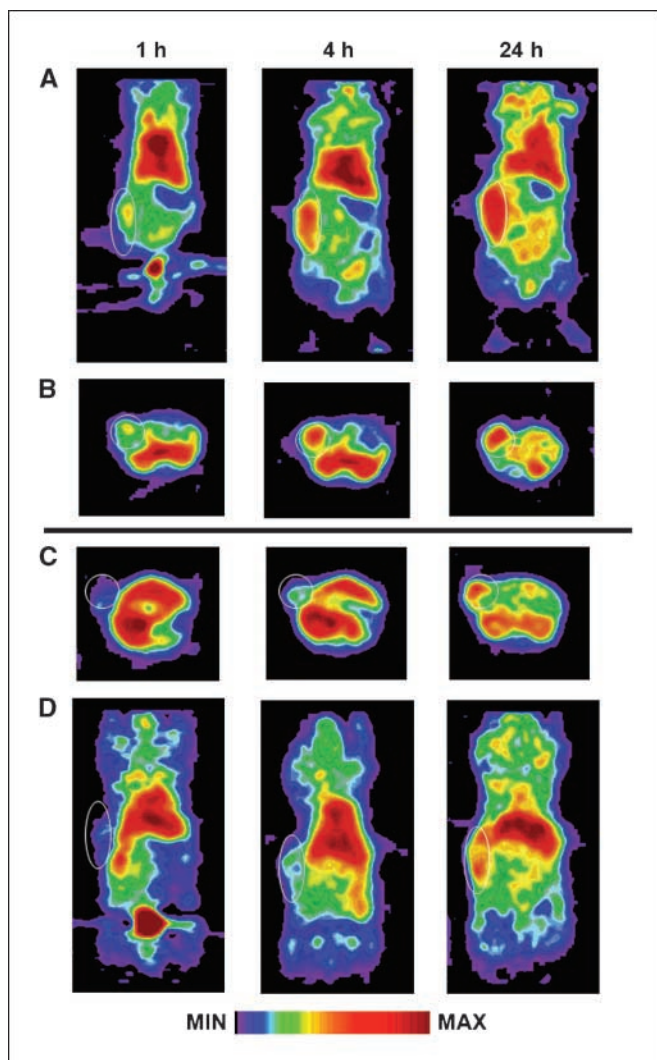*$P < 0.005$, statistical significance between treated and nontreated groups.

As expected, in this experiment, the average pH$_e$ in the non-modulated LNCaP tumors was more acidic than the average pH$_e$ of the tumors in mice having received 7 days of bicarbonated water (6.62 ± 0.35 versus 6.94 ± 0.56, respectively; $P = 0.28$). This correlates well with the data from the biodistribution where ^{64}Cu-DOTA-pHLIP uptake in the nonmodulated LNCaP tumors was greater than the uptake in the tumors in mice having received 7 days of bicarbonated water (4.50 ± 1.71 versus 1.31 ± 0.60, respectively; $P = 0.005$). It should also be noted that the pH$_e$ measured in our MRS experiments is a volume-averaged pH$_e$. Although this measured pH$_e$ provides a good indication of the acidity outside of the cell, it may not reflect the exact pH on the exterior surface of the cells and does not account for tumor heterogeneity. Thus, pH$_e$ as measured by MRS is an indicator, but not a direct measure, of the pH causing insertion.

Discussion

The physiologic differences between normal and tumor tissues provide an opportunity for the development of novel diagnostic and therapeutic agents specifically targeting cancer cells. However, the acidic extracellular environment in tumors has not been properly exploited, probably due to a lack of compounds whose properties change dramatically in the range of pH 6.0 to 7.5. The significance of the current work is that it proposes an innovative and novel method to target tumors based on an intrinsic physiologic property, the acidic extracellular environment, and thereby addresses an important problem in the diagnosis and monitoring or response to therapy of cancer. The method is based on the pH-selective interaction of the pHLIP with cell membranes. In this study, we have shown and validated a novel, pH-selective PET tracer, ^{64}Cu-DOTA-pHLIP. This is the first time a peptide-based PET agent has been employed for the delineation of the pH$_e$ of tumors.

Our data show that ^{64}Cu-DOTA-pHLIP is stable in tumors. None of the animals in any of the studies showed any adverse effects due to the administration of any of the pHLIP constructs. The biodistribution and PET imaging data showed retention of radioactivity in the tumors over 24 h. The tumor uptake of ^{64}Cu-DOTA-pHLIP correlates well with *in vivo* fluorescence imaging studies, which showed that Cy5.5-pHLIP and Alexa 750-pHLIP stayed in tumors for several (>4) days (25). This long retention might be explained by the fact that, when the peptide is inserted into the cell membrane, it is protected from attack by proteases, allowing it to accumulate in tumor tissue in significant amounts.

There were two main factors that might contribute to the accumulation of pHLIP in nontumor tissue. While at normal, physiologic pH, the probability of pHLIP insertion into the cell membrane is low, the peptide still interacts with the surface of the membrane through its hydrophobic motif. Although this produces a small background signal, it also allows for a longer blood circulation of pHLIP, enhancing the probability of delivering functional imaging moieties or therapeutic cargo to the site of disease. The background signal decreases with time, whereas the signal in tumors remains static or is enhanced. A second reason for unwanted background is the relative instability of the ^{64}Cu-DOTA chelation. ^{64}Cu has been shown to dissociate *in vivo* from DOTA and DOTA-conjugates, undergoing subsequent metabolism and trans-chelation to superoxide dismutase and other proteins, resulting in increased accumulation in the blood and liver (27, 34, 35). This could account, in part, for the main differences

Figure 3. Representative small-animal PET image slices of ^{64}Cu-DOTA-pHLIP (200 μCi/animal) in LNCaP (measured tumor pH$_e$, 6.78 ± 0.29) and PC-3 (measured tumor pH$_e$, 7.23 ± 0.10) tumor-bearing mice at various post-injection time points. Differences in tumor SUVs can be visualized by comparing the LNCaP (*A*) coronal and (*B*) transaxial slices to the PC-3 (*C*) transaxial and (*D*) coronal slices. *White circle,* tumor.

accumulate in tumors, consistent with previous fluorescence studies (25). Also, we observed lowering of K-pHLIP level in blood and tissues, although the equivalent mass of labeled K-pHLIP was administered and the data are normalized to the injected dose (%ID/g). We assume that rapid excretion of the K-pHLIP could be associated with its reduced affinity to the membrane at normal pH, in contrast to the parent pHLIP. Our thermodynamic studies indicated that pHLIP has high affinity to the membrane at normal pH (ΔG$_{binding}$ is about −7 kcal/mol at 37°C; ref. 26), which is probably associated with the prolonged peptide circulation in the blood. The pHLIP affinity to the cell membrane increases in an environment of low pH, at which point pHLIP inserts into the membrane and adopts a stable transmembrane configuration. In contrast to pHLIP, the mutant peptide K-pHLIP cannot insert into the cell membrane to form a transmembrane α-helix (25), so it can be assumed that the tumor uptake we observed for ^{64}Cu-DOTA-K-pHLIP in the acute biodistribution studies must be due to the passive diffusion of the construct into the tumor interstitium. Also, as stated, we cannot exclude the possibility that the creation of ^{64}Cu bound to serum proteins by exchange with ^{64}Cu-DOTA-pHLIP contributes to the background, especially at early time points. Therefore, although it is known that K-pHLIP does not target acidity, the use of K-pHLIP may not be an appropriate control system.

The selectivity of the pHLIP was shown by the modulation of pH$_e$ in LNCaP-bearing mice in which more acidic LNCaP tumors had greater uptake of ^{64}Cu-DOTA-pHLIP than the less acidic (bicarb-modulated) LNCaP tumors. As can be seen from Table 2, it is clear that administering sodium bicarbonate significantly altered the uptake of the peptide only in the tumor and kidney. Unlike with K-pHLIP (Table 1), there were no significant differences in the uptake by the skin, which cannot be explained at this time. The use of bicarbonate is known to have a profound effect on pH$_e$ (12, 25, 29). For example, Raghunand and colleagues showed with ^{31}P MRS that the pH$_e$ of MCF-7 human breast cancer xenografts can be effectively and significantly raised with sodium bicarbonate in
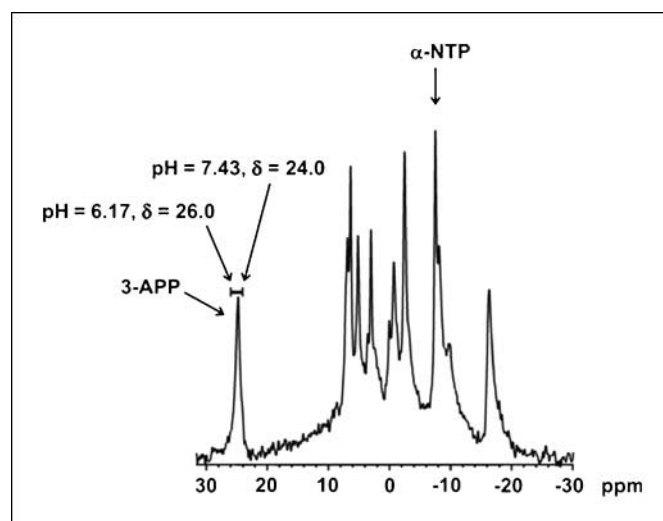
in biodistribution between Cy5-pHLIP and ^{64}Cu-DOTA-pHLIP, particularly the difference in liver uptake. In contrast to the PET results, the fluorescence data showed a very low uptake of Cy5.5-pHLIP by the liver (25), because the NIR dyes were conjugated covalently to the NH$_2$ terminus of the peptide. We therefore believe that the apparent liver uptake of ^{64}Cu-DOTA-pHLIP could be significantly decreased by optimizing the copper-chelating moiety. The cross-bridged cyclam chelator, CBTE2A, has shown improved *in vivo* stability and consequently a reduction in transchelation (35, 36) but requires elevated temperatures for copper complexation that may not compatible with the pHLIP construct.

The control peptide, ^{64}Cu-DOTA-K-pHLIP, which had just two amino acid residues replaced, showed ∼40% less PC-3 tumor uptake as early as 1 h post-injection; we did anticipate that the mutant peptide would have lower uptake in the PC-3 model (the less acidic tumor) than the parent pHLIP. Also, small-animal PET imaging experiments showed that control peptide did not

Figure 4. *In vivo* ^{31}P MRS of a PC-3 tumor. pH$_e$ is estimated from the chemical shift difference (in ppm) between the pH$_e$ indicator 3-APP and the pH-independent chemical shift of α-nucleoside triphosphate (α-*NTP*). The scale bar above the 3-APP resonance indicates a range of chemical shifts (δ) from 24.0 to 26.0 ppm, corresponding to the physiologic range of pH$_e$ (6.17-7.43).

drinking water (12). This was achieved with the mice drinking *ad libitum* water containing 200 mmol/L $NaHCO_3$ for periods up to 90 days continuously, without any changes in subjective parameters and weight gain compared with control mice. In this current study, the average pH_e in the nonmodulated LNCaP tumors was more acidic than the average pH_e of the tumors in mice having received 7 days of bicarbonated water (6.62 ± 0.35 versus 6.94 ± 0.56, respectively; $P = 0.28$). This correlated well with the data from the acute biodistribution where ^{64}Cu-DOTA-pHLIP uptake in the nonmodulated LNCaP tumors was significantly greater that the uptake in the tumors in mice having received 7 days of bicarbonated water (4.50 ± 1.71 versus 1.31 ± 0.60, respectively; $P = 0.005$).

Apart from the liver and blood uptake, the quantitative PET data and images are in general agreement with the biodistribution studies and the previous reported fluorescence studies (25), including uptake of the peptide by the kidney. The kidney has acidic regions and is a major site of catabolism of low molecular weight proteins. The kidney uptake can be reduced by providing mice with bicarbonate-buffered drinking water at pH 8.0 (12, 25, 29) or drugs such as acetozalomide, a carbonic anhydrase inhibitor that causes urinary alkalization. This reduction in kidney uptake with bicarbonate-buffered drinking water was confirmed in our own study presented in Table 2.

In summary, we have synthesized and evaluated the first generation of novel pH_e-sensitive peptide PET agents for the delineation of low pH_e in tumors. This is the first report of this novel class of PET imaging agents. Although the biokinetics of the agent are not optimal, additional strategies are currently under development to enhance tumor accumulation while reducing unwanted background uptake. This first-generation agent offers the possibility of designing a new class of noninvasive pH-selective PET imaging agents that will be useful for the imaging of a broad range of disease states. Multimodal (diagnostic + therapeutic) pHLIP with a NH_2-terminal imaging label and COOH-terminal chemotherapeutic cargo (23) would afford the opportunity to monitor drug delivery, providing a key tool in efforts to predict therapeutic outcome.

Disclosure of Potential Conflicts of Interest

No potential conflicts of interest were disclosed.

Acknowledgments

References

1. Bild AH, Potti A, Nevins JR. Linking oncogenic pathways with therapeutic opportunities. Nat Rev Cancer 2006;6:735–41.
2. Cairns R, Papandreou I, Denko N. Overcoming physiologic barriers to cancer treatment by molecularly targeting the tumor microenvironment. Mol Cancer Res 2006;4:61–70.
3. Coffey DS, Getzenberg RH, DeWeese TL. Hyperthermic biology and cancer therapies. JAMA 2006;296:445–8.
4. Rofstad EK, Mathiesen B, Kindem K, Galappathi K. Acidic extracellular pH promotes experimental metastasis of human melanoma cells in athymic nude mice. Cancer Res 2006;66:6699–707.
5. Stubbs M, McSheehy PM, Griffiths JR. Causes and consequences of acidic pH in tumors: a magnetic resonance study. Adv Enzyme Regul 1999;39:13–30.
6. Gillies RJ. Causes and consequences of hypoxia and acidity in tumors. Trends Mol Med 2001;7:47–9.
7. Raghunand N, Gillies RJ. pH and chemotherapy. Novartis Found Symp 2001;240:199–211.
8. Rajendran JG, Krohn KA. Imaging hypoxia and angiogenesis in tumors. Radiol Clin North Am 2005;43:169–87.
9. Lora-Micheils M, Yu D, Sanders L, et al. Extracellular pH and P-31 magnetic resonance spectroscopic variables are related to outcome in canine soft tissue sarcomas treated with thermoradiotherapy. Clin Cancer Res 2006;12:5733–40.
10. Gerweck LE, Vijayappa S, Kozin S. Tumor pH controls the *in vivo* efficacy of weak acid and base chemotherapeutics. Mol Cancer Therapeutics 2006;5:1275–9.
11. Raghunand N, Gillies RJ. pH and drug resistance in tumors. Drug Resist Update 2000;3:39–47.
12. Raghunand N, He X, van Sluis R, et al. Enhancement of chemotherapy by manipulation of tumour pH. Br J Cancer 1999;80:1005–11.
13. Garcia-Martin ML, Martinez GV, Raghunand N, Sherry AD, Zhang S, Gillies RJ. High resolution pH_e imaging of rat glioma using pH-dependent relaxivity. Magn Reson Med 2006;55:309–15.
14. Bhujwalla ZM, Artemov D, Ballesteros P, Cerdan S, Gillies RJ, Solaiyappan M. Combined vascular and extracellular pH imaging of solid tumors. NMR Biomed 2002;15:114–9.
15. Bhujwalla ZM, McCoy CL, Glickson JD, Gillies RJ, Stubbs M. Estimations of intra- and extracellular volume and pH by ^{31}P magnetic resonance spectroscopy: effect of therapy on RIF-1 tumours. Br J Cancer 1998;78:606–11.
16. Garcia-Martin ML, Hérigault G, Rémy C, et al. Mapping extracellular pH in rat brain gliomas *in vivo* by ^1H magnetic resonance spectroscopic imaging: comparison with maps of metabolites. Cancer Res 2001;61:6524–31.
17. Gallagher FA, Kettunen MI, Day SE, et al. Magnetic resonance imaging of pH *in vivo* using hyperpolarized ^{13}C-labelled bicarbonate. Nat Med 2008;453:940–3.
18. Gillies RJ, Raghunand N, Karcamar GS, Bhujwalla ZM. MRI of the tumor microenvironment. J Magn Reson Imaging 2002;16:430–50.
19. Blower PJ, Lewis JS, Zweit J. Copper radionuclides and radiopharmaceuticals in nuclear medicine. Nucl Med Biol 1996;23:957–80.
20. Lewis JS, Welch MJ, Tang L. Workshop on the production, application and clinical translation of 'non-standard' PET nuclides: a meeting report. Q J Nucl Med Mol Imaging 2008;52:101–6.
21. Anderson CJ, Dehdashti F, Cutler PD, et al. Cu-64-TETA-octreotide as a PET imaging agent for patients with neuroendocrine tumors. J Nucl Med 2001;42:213–21.
22. Vavere AL, Lewis JS. Cu-ATSM: a radiopharmaceutical for the PET imaging of hypoxia. Dalton Trans 2007;43:4893–902.
23. Reshetnyak YK, Andreev OA, Lehnert U, Engelman DM. Translocation of a molecules into cells by pH-dependent insertion of a transmembrane helix. Proc Natl Acad Sci U S A 2006;103:6460–5.
24. Reshetnyak YK, Segala M, Andreev OA, Engelman DM. A monomeric membrane peptide that lives in three worlds: in solution, attached to, and inserted across lipid bilayers. Biophys J 2007;93:2363–72.
25. Andreev OA, Dupuy AD, Segala M, et al. Mechanism and uses of a membrane peptide that targets tumors and other acidic tissues *in vivo*. Proc Natl Acad Sci U S A 2007;104:7893–8.
26. Reshetnyak YK, Andreev OA, Segala M, Markin VS, Engelman DM. Energetics of peptide (pHLIP) binding to and folding across a lipid bilayer membrane. Proc Natl Acad Sci U S A 2008;105:15340–5.
27. Wadas TJ, Wong EH, Weisman GR, Anderson CJ. Copper chelation chemistry and its role in copper radiopharmaceuticals. Curr Pharm Design 2007;13:3–16.
28. McCarthy DW, Shefer RE, Klinkowstein RE, et al. Efficient production of high specific activity ^{64}Cu using a biomedical cyclotron. Nucl Med Biol 1997;24:35–43.
29. Evelhoch JL, Gillies RJ, Karczmar GS, et al. Applications of magnetic resonance in model systems: cancer therapeutics. Neoplasia 2000;2:152–65.
30. Tai YC, Ruangma A, Rowland DJ, et al. Performance evaluation of the microPET focus: a third-generation microPET scanner dedicated to animal imaging. J Nucl Med 2005;46:455–63.
31. Gillies RJ, Liu Z, Bhujwalla Z. ^{31}P-MRS measurements of extracellular pH of tumors using 3-aminopropyl-phosphonate. Am J Physiol 1994;267:C195–203.
32. Bretthorst G. Bayesian analysis. III. Applications to NMR signal detection, model selection, and parameter estimation. J Magn Reson 1990;88:571–95.
33. Ackerman JJH, Soto GE, Spees WM, Zhu Z, Evelhoch JL. The NMR chemical shift pH measurement revisited: analysis of error and modeling of a pH dependent reference. Magn Reson Med 1996;36:674–83.
34. Boswell CA, Sun X, Niu W, et al. Comparative *in vivo* stability of copper-64-labeled cross-bridged and conventional tetraazamacrocyclic complexes. J Med Chem 2004;47:1465–74.
35. Sprague JE, Peng Y, Sun X, et al. Preparation and biological evaluation of copper-64-labeled Tyr^3-octreotate using a cross-bridged macrocyclic chelator. Clin Cancer Res 2004;10:8674–82.
36. Wei L, Butcher C, Miao Y, et al. Synthesis and biological evaluation of Cu-64 labeled rhenium-cyclized α-MSH peptide analog using a cross-bridged cyclam chelator. J Nucl Med 2007;48:64–72.